

# Advanced control scheme of doubly fed induction generator for wind turbine using second sliding mode control

Hafida Bekouche<sup>1,2</sup>, Abdelkader Chaker<sup>1,2</sup>

<sup>1</sup>Department of Electrical Engineering, National School of Polytechnics Oran (ENPO), Oran, Algeria

<sup>2</sup>Simulation, Commande, Analyse et Maintenance des Réseaux Electriques (SCAMRE) Laboratory, Oran, Algeria

## Article Info

### Article history:

Received Jan 3, 2022

Revised Feb 19, 2023

Accepted Mar 7, 2023

### Keywords:

Active power

Doubly fed induction generator

Proportional integral

Reactive power

Second order sliding mode

controller

Sliding mode controller

Wind turbine

## ABSTRACT

This paper describes a speed control device for generating electrical energy on an electricity network based on the doubly fed induction generator (DFIG) used for wind power conversion systems. At first, a double-fed induction generator model was constructed. A control law is formulated to govern the flow of energy between the stator of a DFIG and the energy network using three types of controllers: proportional integral (PI), sliding mode controller (SMC) and second order sliding mode controller (SOSMC). Their different results in terms of power reference tracking, reaction to unexpected speed fluctuations, sensitivity to perturbations, and resilience against machine parameter alterations are compared. MATLAB/Simulink was used to conduct the simulations for the preceding study. Multiple simulations have shown very satisfying results, and the investigations demonstrate the efficacy and power-enhancing capabilities of the suggested control system.

*This is an open access article under the [CC BY-SA](https://creativecommons.org/licenses/by-sa/4.0/) license.*



## Corresponding Author:

Hafida Bekouche

Department of Electrical Engineering, National School of Polytechnics Oran (ENPO)

Simulation, Commande, Analyse et Maintenance des Réseaux Electriques (SCAMRE) Laboratory

Oran, Algeria

Email: hafidabekouche2@gmail.com

## 1. INTRODUCTION

Recently, the field of wind energy technology has garnered significant attention from both the scientific community and industry, leading to a substantial body of scientific work within this timeframe. The wind turbine systems (WTS) that utilize a doubly fed induction generator (DFIG) and operate at variable speeds are notably prevalent in terrestrial wind farms [1]. Distinct from other generators employed in variable speed WTS, the rotor-side converter in the DFIG is specifically engineered to handle only 30% of the total rated power.

This aspect stands as the principal advantage of employing a DFIG, effectively leading to a reduction in the cost associated with the converter [2]. Despite the DFIG presenting numerous advantages, the complexity of its multivariable control system design poses significant challenges. The literature is replete with various control schemes for DFIG across different applications within the power system. Among these, the sliding mode control (SMC) strategy has emerged as the foremost choice in recent times for the robust regulation of nonlinear dynamic systems. A series of studies focusing on the SMC application for DFIG underscores its popularity [3]–[5]. Nonetheless, a notable limitation of this control strategy is the chatter phenomenon, which arises due to the control's intermittent nature. To address this limitation, various enhancements to the conventional control methodology have been introduced, with the boundary layer technique standing out as particularly noteworthy [6]–[8].

This study focuses on managing the transfer of electrical power between the stator of the DFIG and the electrical grid, facilitating independent control over both active and reactive power. The management of these power types, active and reactive, is executed utilizing proportional-integral (PI), sliding mode control (SMC), and second order sliding mode control (SOSMC) approaches. The performance of these strategies is evaluated in terms of their ability to accurately follow reference signals, their resilience to perturbations, and their general reliability.

## 2. MODEL OF DFIG

The mathematical formulation of DFIG closely resembles that of a conventional induction motor, with the key difference being the inclusion of a non-zero voltage across the rotor. Park transformation framework of DFIG is widely referenced in academic literature [8]–[10]. The principal equations governing the stator and rotor dynamics of DFIG within the Park coordinate system are outlined as (1).

$$\begin{cases} V_{ds} = R_s I_{ds} + \frac{d}{dt} \psi_{ds} - \omega_s \psi_{qs} \\ V_{qs} = R_s I_{qs} + \frac{d}{dt} \psi_{qs} + \omega_s \psi_{ds} \\ V_{dr} = R_r I_{dr} + \frac{d}{dt} \psi_{dr} - \omega_r \psi_{qr} \\ V_{qr} = R_r I_{qr} + \frac{d}{dt} \psi_{qr} + \omega_r \psi_{dr} \end{cases}, \quad \begin{cases} \psi_{ds} = L_s I_{ds} + M I_{dr} \\ \psi_{qs} = L_s I_{qs} + M I_{qr} \\ \psi_{dr} = L_r I_{dr} + M I_{ds} \\ \psi_{qr} = L_r I_{qr} + M I_{qs} \end{cases} \quad (1)$$

These equations encompass voltages ( $V_{dr}$ ,  $V_{qr}$ ,  $V_{ds}$ , and  $V_{qs}$ ), currents ( $I_{dr}$ ,  $I_{qr}$ ,  $I_{ds}$ , and  $I_{qs}$ ), and flux linkages ( $\psi_{dr}$ ,  $\psi_{qr}$ ,  $\psi_{ds}$ , and  $\psi_{qs}$ ) associated with both the rotor and stator.  $R_r$  and  $R_s$  denote the resistance of the rotor and stator windings, respectively, whereas  $L_r$  and  $L_s$  are inductances of the rotor and stator, with  $M$  signifying inductance between two coils.

Additionally, the relationship linking the stator and rotor electrical frequencies to mechanical speed is expressed by:  $\omega_s = \omega_r + \omega$ . In this equation,  $\omega_r$  and  $\omega_s$  denote the electrical frequencies of the rotor and stator, respectively, while  $\omega$  represents the mechanical frequency.

$$C_{em} = C_r + J \cdot \frac{d\Omega}{dt} + F_r \cdot \Omega \quad (2)$$

Electromagnetic torque,  $C_{em}$ , can be articulated as (1).

$$C_{em} = \frac{3}{2} n_p \frac{M}{L_s} (\psi_{qs} I_{dr} - \psi_{ds} I_{qr}) \quad (3)$$

In this context,  $C_r$  denotes load torque,  $\Omega$  signifies rotational speed of mechanical rotor,  $F_r$  represents coefficient of viscous friction,  $n_p$  is count of pole pairs, and  $J$  indicates moment of inertia. For the stator, the definitions of reactive and active power are given as (4).

$$\begin{cases} P_s = \frac{3}{2} (I_{ds} V_{ds} + I_{qs} V_{qs}) \\ Q_s = \frac{3}{2} (I_{ds} V_{qs} - I_{qs} V_{ds}) \end{cases} \quad (4)$$

Using a Park reference frame oriented along the stator flux enables independent control of stator's active and reactive power. Aligning d-axis with the stator flux vector and taking into account (1), while disregarding  $R_s$ , leads to the derivation of the formula:

$$\psi_{qs} = 0 \text{ and } \psi_{ds} = \psi_s \quad (5)$$

$$\begin{cases} V_{qs} = \omega_s \psi_s \\ V_{ds} = 0 \end{cases} \quad (6)$$

$$\begin{cases} I_{ds} = \frac{\psi_s}{L_s} - \frac{M}{L_s} I_{dr} \\ I_{qs} = -\frac{M}{L_s} I_{qr} \end{cases} \quad (7)$$

Using (6) and (7), the following expression may be derived for (4):

$$\begin{cases} P_s = -\frac{3}{2} \frac{\omega_s \psi_s M}{L_s} I_{qr} \\ Q_s = -\frac{3}{2} \left( \frac{\omega_s \psi_s M}{L_s} I_{dr} - \frac{\omega_s \psi_s^2}{L_s} \right) \end{cases} \quad (8)$$

Therefore, the formulation for the electromagnetic torque can be expressed in the subsequent manner:

$$C_{em} = -\frac{3}{2} n_p \frac{M}{L_s} I_{qr} \psi_{ds} \quad (9)$$

### 3. CONTROLLERS SYNTHESIS

This segment of the study embarks on a comparative analysis of DFIG performance when regulated by PI, SMC, and SOSMC. A diagrammatic depiction of the control system, as showcased in Figure 1, is based on the relationships outlined in (7) and (8). The elements denoted as  $R_1, R_2, R_3,$  and  $R_4$  are associated with the controllers for rotor currents and stator power, respectively.

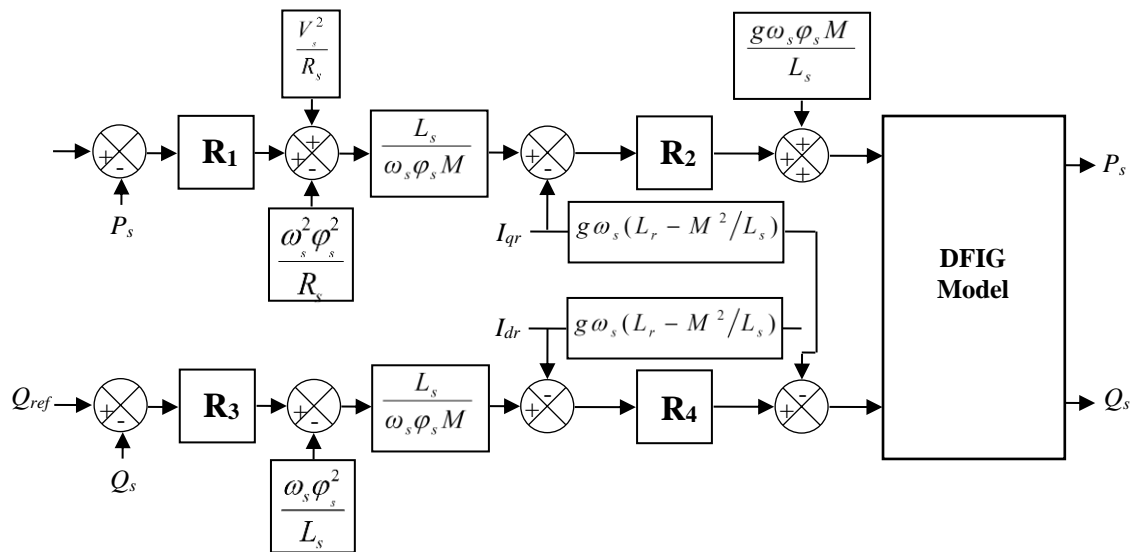


Figure 1. Power control of the DFIG

#### 3.1. PI regulator synthesis

The setup of the PI controller is noted for its simplicity in implementation. The variables  $k_i$  and  $k_p$  signify the integral and proportional gains, correspondingly. The controlled transfer function is denoted as  $B/A$ , with  $A$  and  $B$  being defined by (10).

$$A = L_s R_r + L_s \cdot p \left( L_r - \frac{M^2}{L_s} \right) \text{ and } B = M \omega_s \psi_s \quad (10)$$

The parameters for the regulator are established through a pole compensation strategy [11]. The response time for the regulated system is designed to be 10 milliseconds, deemed adequate for the intended application, as a shorter duration may lead to transients with significant overshoot. The derived values are presented as (11):

$$k_i = 1000 \frac{L_s R_r}{\omega_s \psi_s M} \text{ and } k_p = 1000 \frac{L_s \left( L_r - \frac{M^2}{L_s} \right)}{\omega_s \psi_s M} \quad (11)$$

It is pertinent to mention that alternative methodologies exist for calculating a standard PI regulator, yet pole compensation offers a straightforward application via a first-order transfer function, making it apt for comparative analyses in this context.

**3.2. Sliding mode controller**

SMC emerges as a formidable nonlinear control mechanism, lauded for bestowing an invariance property against uncertainties on system dynamics, making it exceedingly resilient [12]–[14]. The quintessence of SMC lies in its capacity to direct system errors towards a predefined switching surface. A process decomposed into three integral components as depicted in Figure 2.

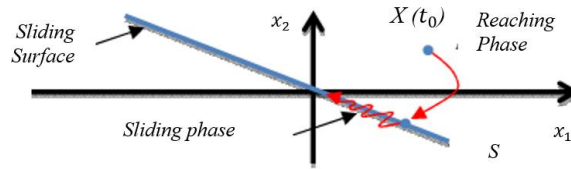


Figure 2. Phase portrait of sliding mode control

**3.2.1. Choice of switching surface**

The construction of a control system tailored for nonlinear systems, outlined in canonical form, is explicated in (12) [15].

$$\begin{cases} \dot{x} = B(x, t)V(x, t) + f(x, t) \\ V \in Rm, x \in Rn, \text{ran}(B(x, t)) = m \end{cases} \tag{12}$$

Here:  $B(x, t)$ ;  $f(x, t)$  denote two continuous, albeit unknown, nonlinear functions presumed to be bounded. To ascertain sliding surface, the framework introduced by studies [16], [17] is employed.

$$S(X) = \left(\frac{d}{dt} + \lambda\right)^{n-1} e; e = x^* - x \tag{13}$$

$e, \lambda, n, x^*$ , and  $x$  representing error in signal to be corrected, a positive scalar, the system's order, the target signal, and the control signal's state variable, respectively.

**3.2.2. Convergence condition**

The convergence criterion towards the sliding surface is determined by the Lyapunov stability theorem [18]. The theorem guarantees the surface's attractiveness and invariance.

$$S \cdot \dot{S} < 0 \tag{14}$$

**3.2.3. Calculation of control**

The control strategy is delineated in (15) [12].

$$V^{com} = V^{eq} + V^n \tag{15}$$

In (15),  $V^{eq}$ ,  $V^{com}$  and  $V^n$  signify the equivalent control vector, the composite control vector, and the corrective factor, respectively. These components must be computed to fulfill the stability prerequisites of the chosen control approach.

$$V^n = K \text{sat}(S(X)/\delta) \tag{16}$$

$$\text{sat}(S(X)/\delta) = \begin{cases} \text{sign}(S) & \text{if } |S| > \delta \\ S/\delta & \text{if } |S| < \delta \end{cases} \tag{17}$$

The function,  $\text{sat}((S(x)/\delta)$  introduces a saturation function, with  $\delta$  indicating boundary layer's thickness: Discrepancy among actual and reference stator powers is designated as the sliding mode surface, leading to the development of the (18):

$$\begin{cases} S_d = P_{s-ref} - P_s \\ S_q = Q_{s-ref} - Q_s \end{cases} \tag{18}$$

Differentiation of (18) provides:

$$\begin{cases} \dot{S}_d = \dot{P}_{s-ref} - \dot{P}_s \\ \dot{S}_q = \dot{Q}_{s-ref} - \dot{Q}_s \end{cases} \quad (19)$$

By incorporating the power expressions from (8) into (19), the resultant equation is obtained.

$$\begin{cases} \dot{S}_d = \dot{P}_{s-ref} - \frac{\omega_s \psi_s M}{L_s} i_{qr} \\ \dot{S}_q = \dot{Q}_{s-ref} + \frac{\omega_s \psi_s M}{L_s} i_{dr} - \frac{\omega_s \psi_s^2}{L_s} \end{cases} \quad (20)$$

The control vector components,  $V_{dr}$  and  $V_{qr}$ , are pivotal in guiding the system's convergence towards the targeted state. The computation of the control vector  $V_{dqeq}$  is achieved by imposing  $\dot{S}_{dq} = 0$  ensuring equivalence of control elements, as specified by (21).

$$\begin{cases} V_{rq}^{eq} = \frac{L_s}{\omega_s \psi_s M} \dot{P}_{s-ref} + R_r I_{rq} - (L_r - \frac{M^2}{L_s}) g \omega_s I_{rd} + \frac{g \omega_s \psi_s M}{L_s} + \frac{L_s (V_s^2 - \omega_s^2 \psi_s^2)}{\omega_s \psi_s M R_s} \\ V_{rd}^{eq} = \frac{L_s (L_r - \frac{M^2}{L_s})}{\omega_s \psi_s M} \dot{Q}_{s-ref} + R_r I_{rd} - (L_r - \frac{M^2}{L_s}) g \omega_s I_{rq} + \frac{(L_r - \frac{M^2}{L_s}) \psi_s}{M} \end{cases} \quad (21)$$

For enhanced performance in terms of surface dynamics and commutation, the control vector is defined according to the following specification [8]:

$$\begin{cases} V_{rq}^n = K_1 \cdot \text{sign}(S_d) \\ V_{rd}^n = K_2 \cdot \text{sign}(S_q) \end{cases} \quad (22)$$

The presence of sliding mode depends on meeting specific criteria:  $S \cdot \dot{S} < 0$

### 3.3. Second order sliding mode controller (SOSMC)

SOSMC is a sophisticated control strategy renowned for its robustness against system perturbations and uncertainties. Despite the efficacy of SMC, its direct implementation can induce chatter, a phenomenon with potentially detrimental effects on control actuators and the introduction of undesired dynamics. SOSMC methodology addresses these issues by extending the conventional sliding mode principle to the higher-order derivatives of sliding manifold [19], rather than focusing solely on initial derivative as in traditional SMC. This modification significantly diminishes chatter, preserving the intrinsic benefits of SMC.

SOSMC framework guarantees the alignment of active and reactive powers with their respective reference values. Extensive investigations have explored diverse SOSMC algorithms, particularly emphasizing output feedback [20]–[23]. Derived from the established sliding mode surface (20), the following expressions can be inferred:

$$\begin{cases} \dot{S}_d = \dot{P}_{s-ref} - \frac{\omega_s \psi_s M}{L_s} i_{qr} \\ \ddot{S}_d = Y_1(t, x) + \Lambda_1(t, x) I_{qr} \end{cases} \quad (23)$$

and

$$\begin{cases} \dot{S}_q = \dot{Q}_{s-ref} + \frac{\omega_s \psi_s M}{L_s} i_{dr} - \frac{\omega_s \psi_s^2}{L_s} \\ \ddot{S}_q = Y_2(t, x) + \Lambda_2(t, x) I_{dr} \end{cases} \quad (24)$$

Within this context,  $Y_1(t, x)$ ,  $Y_2(t, x)$ ,  $\Lambda_1(t, x)$  and  $\Lambda_2(t, x)$  are uncertain variables that fulfill:

$$\begin{cases} Y_1 > 0, |Y_1| > \lambda, 0 < K_m < \Lambda_1 < K_M \\ Y_2 > 0, |Y_2| > \lambda, 0 < K_m < \Lambda_2 < K_M \end{cases} \quad (25)$$

The suggested high order (SMC) is based on the super twisting algorithm published by Levant in [24] and consists of two components [25]:

$$V_{rq} = v_1 + v_2 \tag{26}$$

with

$$\begin{aligned} V_1 &= -k_1 \cdot \text{sign}(S_d) \\ v_2 &= -l \cdot |S|^\gamma \cdot \text{sign}(S_d) \\ V_{rd} &= w_1 + w_2 \end{aligned} \tag{27}$$

with

$$\begin{aligned} W_1 &= -k_2 \cdot \text{sign}(S_q) \\ w_2 &= -l \cdot |S_q|^\gamma \cdot \text{sign}(S_q) \end{aligned}$$

The super twisting algorithm, a fundamental component of the proposed high order sliding mode control strategy, as elucidated by Levant. The decomposition into two key components, further elaborating the control mechanism's operational dynamics.

$$\begin{cases} k_i > \frac{\lambda_i}{K_{mi}} \\ l_i^2 \geq \frac{K_{mi}(k_i + \lambda_i)}{K_{mi}(k_i - \lambda_i)} \frac{4\lambda_i}{K_{mi}^2}; i = 1,2 \\ 0 < \gamma \leq 0.5 \end{cases}$$

#### 4. RESULTS AND DISCUSSION

The examination segment delves into simulations conducted on a 1.5 MW generator integrated into a 398 V/50 Hz electrical network. To assess the efficacy of the three controller designs: PI, SMC, and SOSMC. The investigation encompasses a trio of tests: tracking performance, sensitivity to speed variations, and adaptability to changes in machine parameters.

##### 4.1. Tracking test

This evaluation emphasizes the fundamental tracking performance of the PI and SMC controllers via simulation, as depicted in Figure 3. The illustration demonstrates that both controllers closely follow their designated active and reactive power references. However, it is notable that the PI controller exhibits a discernible lag in its response relative to SMC, showcasing latter's superior performance in this test.

The harmonic spectrum of the stator current for each controller, derived via FFT, is represented in Figure 4. Comparative analysis reveals that the total harmonic distortion (THD) values for PI and SMC controllers are 2.01% and 2.09% respectively, as shown in Figures 4(a) and 4(b). Whereas the SOSMC features a reduced THD of 1.9% in Figure 4(c), highlighting SOSMC as the most effective strategy for mitigating chatter issues. Despite the advancements with SOSMC, the torque THD remains relatively high, a consequence attributed to the necessity of dual power converters; a notable drawback of DFIG configuration.

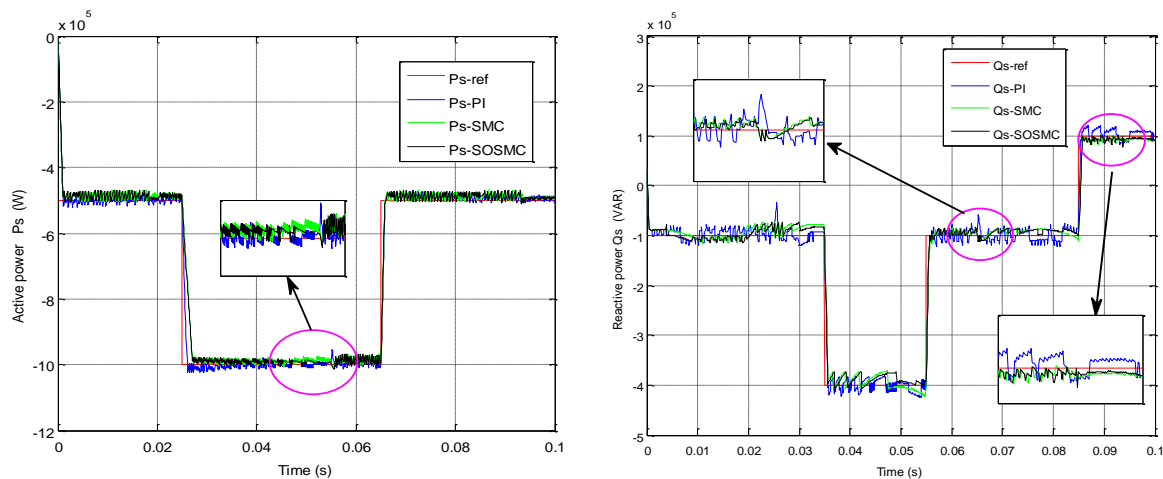


Figure 3. Reference tracking test

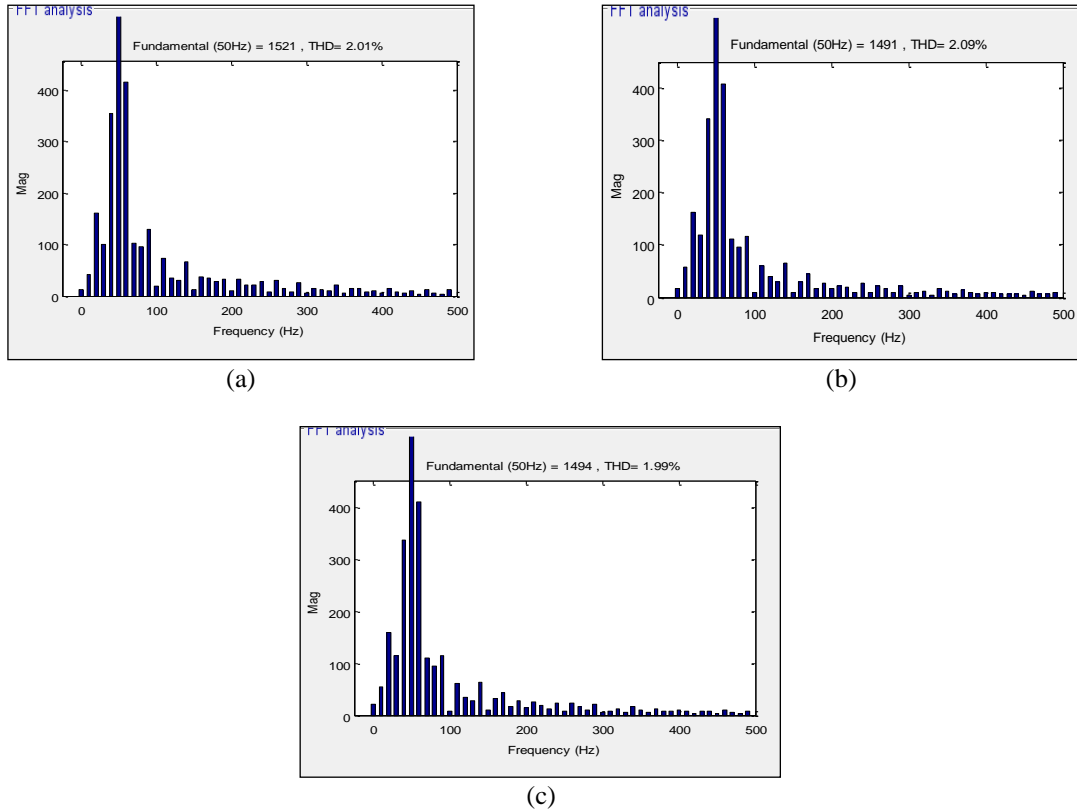


Figure 4. Harmonic spectrum of single-phase stator current for (a) PI, (b) SMC, and (c) SOSMC

**4.2. Speed variation sensitivity test**

This particular test aims to evaluate the effect of changes in DFIG speed on the active and reactive power outputs. Speed adjustment was simulated at time = 0.05s, transitioning from 150 to 170 rad/s. Results depicted in Figure 5 demonstrate that such a speed alteration induced significant oscillations in the power curves when employing a fuzzy logic controller (FLC). Conversely, the impact on the system controlled by an SMC was considerably less pronounced. Remarkably, SMC showcased almost impeccable rejection of speed disturbances, with only minor power fluctuations (under 3%) observed. This characteristic is particularly advantageous for wind power applications, ensuring the stability and quality of electricity generation amidst wind speed variations.

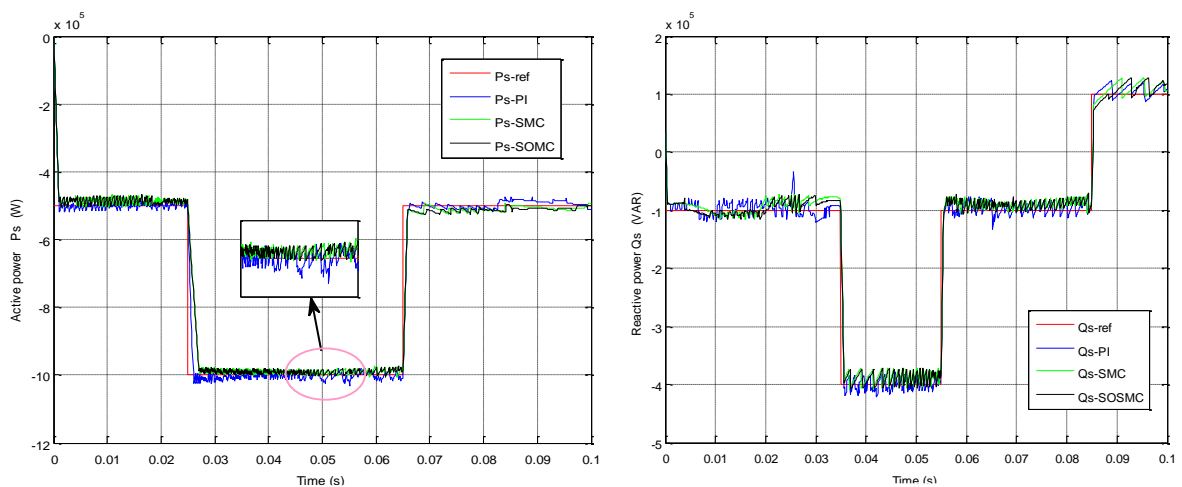


Figure 5. Speed variation sensitivity analysis

### 4.3. Robustness

In the robustness assessment, variations were introduced to the machine parameters. Specifically, the resistances of the stator and rotor ( $R_s$  and  $R_r$ ) were doubled, while the inductances ( $L_s$ ,  $L_r$ , and  $M$ ) were halved. These adjustments were made while keeping the equipment operating under standard conditions. The outcomes, presented in Figure 6, indicate that changes in DFIG parameters significantly affect the power curves. The impact was more pronounced for systems controlled by FLC compared to those managed by SMC controllers, underscoring the superior resilience of the latter.

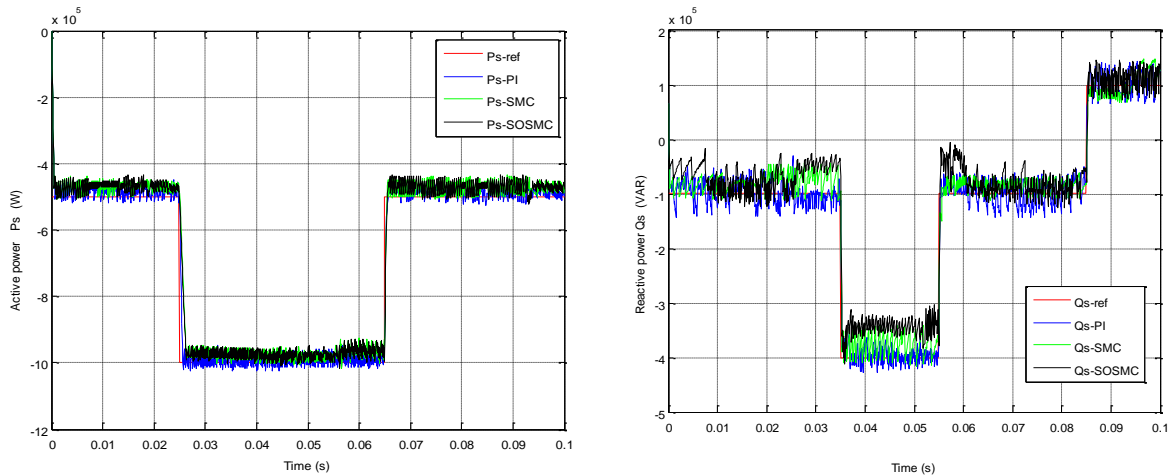


Figure 6. Impact of variations in machine parameters on DFIG control

## 5. CONCLUSION

In this research, we introduce an innovative robust control approach utilizing variable-speed wind turbine (VST) in conjunction with a doubly-fed induction generator (DFIG). The study unfolds in three pivotal phases, beginning with an analytical exploration of the vector-controlled matrix converter. Following this, a vector control (VC) strategy is implemented to separate the magnetic flux from the electromagnetic torque, allowing the DFIG to function similarly to a DC motor. The study reaches its apex by controlling the stator's active and reactive power outputs, achieved through the development and comparative evaluation of four different controller modalities. The simulations underscore the SOSMC's exceptional ability to counteract variations in system parameters and loads, ensuring precise speed control throughout fluctuating conditions without leading to overshoot, thereby achieving decoupling, stability, and balance. When contrasted with other SMC techniques, the SOSMC stands out, particularly for its efficacy in curbing chattering phenomena. Although torque levels are subject to high-frequency oscillations due to the inverter's inherent characteristics and the control's variable structure, the adoption of a second-order sliding mode and elevated modulation index markedly reduces these fluctuations. Furthermore, this control methodology is distinguished by its ease of implementation through software programming, offering a practical and effective solution for enhancing DFIG system robustness and functionality.

## REFERENCES




- [1] A. Kerboua and M. Abid, "Hybrid fuzzy sliding mode control of a doubly-fed induction generator speed in wind turbines," *Journal of Power Technologies*, vol. 95, no. 2, pp. 126–133, 2015.
- [2] Y. Sahri et al., "New intelligent direct power control of DFIG-based wind conversion system by using machine learning under variations of all operating and compensation modes," *Energy Reports*, vol. 7, pp. 6394–6412, Nov. 2021, doi: 10.1016/j.egy.2021.09.075.
- [3] M. I. Martinez, A. Susperregui, G. Tapia, and H. Camblong, "Sliding-mode control for a DFIG-based wind turbine under unbalanced voltage," *IFAC Proceedings Volumes (IFAC-PapersOnline)*, vol. 44, no. 1 PART 1, pp. 538–543, Jan. 2011, doi: 10.3182/20110828-6-IT-1002.00854.
- [4] R. Ruiz, E. N. Sánchez, and A. G. Loukianov, "Real-time sliding mode control for a doubly fed induction generator," in *Proceedings of the IEEE Conference on Decision and Control*, Dec. 2011, pp. 2975–2980, doi: 10.1109/CDC.2011.6160470.
- [5] S. Ebrahimkhani, "Robust fractional order sliding mode control of doubly-fed induction generator (DFIG)-based wind turbines," *ISA Transactions*, vol. 63, pp. 343–354, Jul. 2016, doi: 10.1016/j.isatra.2016.03.003.
- [6] J. López, P. Sanchis, X. Roboam, and L. Marroyo, "Dynamic behavior of the doubly fed induction generator during three-phase voltage dips," *IEEE Transactions on Energy Conversion*, vol. 22, no. 3, pp. 709–717, Sep. 2007, doi: 10.1109/TEC.2006.878241.
- [7] F. Cupertino, D. Naso, E. Mininno, and B. Turchiano, "Sliding-mode control with double boundary layer for robust compensation






- of payload mass and friction in linear motors,” *IEEE Transactions on Industry Applications*, vol. 45, no. 5, pp. 1688–1696, 2009, doi: 10.1109/TIA.2009.2027521.
- [8] A. Fekik, H. Denoun, M. L. Hamida, A. T. Azar, M. Atig, and Q. M. Zhu, “Neural network based switching state selection for direct power control of three phase PWM-rectifier,” *2018 10th International Conference on Modelling, Identification and Control (ICMIC)*, Guiyang, China, 2018, pp. 1-6, doi: 10.1109/ICMIC.2018.8529997.
- [9] K. Kerrouche, A. Mezouar, and K. Belgacem, “Decoupled control of doubly fed induction generator by vector control for wind energy conversion system,” *Energy Procedia*, vol. 42, pp. 239–248, 2013, doi: 10.1016/j.egypro.2013.11.024.
- [10] K. Narimene, M. Kheira, and F. Mohamed, “Robust neural control of wind turbine based doubly fed induction generator and NPC three level inverter,” *Periodica polytechnica Electrical engineering and computer science*, vol. 66, no. 2, pp. 191–204, May 2022, doi: 10.3311/PPee.19921.
- [11] G. S. Kaloi, J. Wang, and M. H. Baloch, “Active and reactive power control of the doubly fed induction generator based on wind energy conversion system,” *Energy Reports*, vol. 2, pp. 194–200, Nov. 2016, doi: 10.1016/j.egypro.2016.08.001.
- [12] R. J. Wai and J. M. Chang, “Implementation of robust wavelet-neural-network sliding-mode control for induction servo motor drive,” *IEEE Transactions on Industrial Electronics*, vol. 50, no. 6, pp. 1317–1334, Dec. 2003, doi: 10.1109/TIE.2003.819570.
- [13] V. I. Utkin, “Sliding mode control design principles and applications to electric drives,” *IEEE Transactions on Industrial Electronics*, vol. 40, no. 1, pp. 23–36, Feb. 1993, doi: 10.1109/41.184818.
- [14] K. J. Astrom, and B. Wittenmark, *Adaptive control*. New York: Addison-Wesley, 1995.
- [15] T. Sun, Z. Chen, and F. Blaabjerg, “Flicker study on variable speed wind turbines with doubly fed induction generators,” *IEEE Transactions on Energy Conversion*, vol. 20, no. 4, pp. 896–905, Dec. 2005, doi: 10.1109/TEC.2005.847993.
- [16] J. J. E. Slotine and W. Li, *Applied nonlinear control*. Englewood cliffs, NJ, 1991.
- [17] J. J. E. Slotine, “Sliding controller design for non-linear systems,” *International Journal of Control*, vol. 40, no. 2, pp. 421–434, Aug. 1984, doi: 10.1080/00207178408933284.
- [18] A. Hinda, M. Khiat, and Z. Boudjema, “Advanced control scheme of a unified power flow controller using sliding mode control,” *International Journal of Power Electronics and Drive Systems (IJPEDS)*, vol. 11, no. 2, pp. 625–633, Jun. 2020, doi: 10.11591/ijpeds.v11.i2.pp625-633.
- [19] M. L. Tseng and M. S. Chen, “Chattering reduction of sliding mode control by low-pass filtering the control signal,” *Asian Journal of Control*, vol. 12, no. 3, pp. 392–398, Feb. 2010, doi: 10.1002/asjc.195.
- [20] G. B. Koo, J. B. Park, and Y. H. Joo, “Decentralized fuzzy observer-based output-feedback control for nonlinear large-scale systems: An LMI approach,” *IEEE Transactions on Fuzzy Systems*, vol. 22, no. 2, pp. 406–419, Apr. 2014, doi: 10.1109/TFUZZ.2013.2259497.
- [21] Y. W. Tsai and V. Van Huynh, “A multitask sliding mode control for mismatched uncertain large-scale systems,” *International Journal of Control*, vol. 88, no. 9, pp. 1911–1923, Apr. 2015, doi: 10.1080/00207179.2015.1025293.
- [22] H. Wu, S. Liu, C. Cheng, and C. Du, “Observer based direct adaptive fuzzy second-order-like sliding mode control for unknown nonlinear systems,” *Proceedings of the Institution of Mechanical Engineers, Part E: Journal of Process Mechanical Engineering*, vol. 235, no. 2, pp. 197–207, Aug. 2021, doi: 10.1177/0954408920952595.
- [23] C. T. Nguyen, C. T. Hien, and V. D. Phan, “Single phase second order sliding mode controller for complex interconnected systems with extended disturbances and unknown time-varying delays,” *International Journal of Electrical and Computer Engineering (IJECE)*, vol. 12, no. 5, pp. 4852–4860, Oct. 2022, doi: 10.11591/ijece.v12i5.pp4852-4860.
- [24] A. Levant and L. Alelishvili, “Integral high-order sliding modes,” *IEEE Transactions on Automatic Control*, vol. 52, no. 7, pp. 1278–1282, Jul. 2007, doi: 10.1109/TAC.2007.900830.
- [25] S. Benelghali, M. E. H. Benbouzid, J. F. Charpentier, T. Ahmed-Ali, and I. Munteanu, “Experimental validation of a marine current turbine simulator: Application sliding mode control,” *IEEE Transactions on Industrial Electronics*, vol. 58, no. 1, pp. 118–126, Jan. 2011, doi: 10.1109/TIE.2010.2050293.

## AUTHORS BIOGRAPHIES



**Hafida Bekouche**    In 2014, he earned a Master of Science Ecole Nationale polytechnique d’oran Maurice Audin, Algeria. Today, he is a doctoral student at the same institution. His research interests include robust control techniques, power transmission protection, particle swarm optimization, power distribution protection, and alternative energy sources. She can be contacted at email: hafidabekouche2@gmail.com.



**Abdelkader Chaker**    In 2002, he earned a Ph.D. in engineering systems from the University of Saint Petersburg. Today, he is a professor at the Electrical Engineering Department of the Ecole Nationale polytechnique d’oran Maurice Audin, Algeria. Control of huge power systems, multimachine multiconverter systems, and unified power-flow He can be contacted at email: chakera@yahoo.fr.